

PENNSYLVANIA STATE



45223

1N-28-011

146046

P-47

PROPULSION ENGINEERING RESEARCH CENTER

IGNITION AND COMBUSTION CHARACTERISTICS OF
METALLIZED PROPELLANTS

Semi-Annual Report
(January - June 1991)

Prepared by
D. C. Mueller and S. R. Turns

for

NASA Lewis Research Center
Grant No. NAG 3-1044

N93-20231

Unclas

G3/28 0146046

A UNIVERSITY SPACE ENGINEERING RESEARCH CENTER

TR-91-008

106 RESEARCH BUILDING EAST
UNIVERSITY PARK, PENNSYLVANIA 16801

(NASA-CR-192231) IGNITION AND
COMBUSTION CHARACTERISTICS OF
METALLIZED PROPELLANTS Semiannual
Report, Jan. - Jun. 1991
(Pennsylvania State Univ.) 47 p



**IGNITION AND COMBUSTION CHARACTERISTICS OF
METALLIZED PROPELLANTS**

**Semi-Annual Report
(January 1991-June 1991)**

Prepared by

D. C. Mueller and S. R. Turns

**Department of Mechanical Engineering
and the
Propulsion Engineering Research Center
The Pennsylvania State University
University Park, Pa 16802**

for

NASA Lewis Research Center

Grant No. NAG 3-1044

**Bryan Palaszewski
NASA Technical Officer**

September 1991

SUMMARY

Over the past six months, experimental investigations were continued and theoretical work on the secondary atomization process was begun . Final shakedown of the sizing/velocity measuring system was completed and the aluminum combustion detection system was modified and tested. Atomizer operation was improved to allow steady state operation over long periods of time for several slurries. To validate the theoretical modeling, work involving carbon slurry atomization and combustion was begun and qualitative observations were made. Simultaneous measurements of aluminum slurry droplet size distributions and detection of burning aluminum particles were performed at several axial locations above the burner. The principle theoretical effort was the application of a rigid shell formation model to aluminum slurries and an investigation of the effects of various parameters on the shell formation process. This shell formation model was extended to include the process leading up to droplet disruption, and previously developed analytical models were applied to yield theoretical aluminum agglomerate ignition and combustion times. The several theoretical times were compared with the experimental results.

TABLE OF CONTENTS

SUMMARY	1
OVERALL PROGRAM OBJECTIVES	3
PROGRESS DURING REPORTING PERIOD	4
OVERVIEW	4
THEORETICAL EFFORTS	4
Disruptive Burning Model Concepts	4
Rigid Shell Formation	5
Disruption	11
Pressure Build-up	16
Brittle Shell Failure	19
Model Results	19
EXPERIMENTAL EFFORTS	23
Aluminum Combustion Detection	25
Slurry Atomization	28
Combustion and Ignition Tests	30
Test Objectives	30
Carbon Slurries	30
Aluminum Slurries	31
Test Conditions	31
Results	33
COMPARISON OF EXPERIMENTAL AND THEORETICAL RESULTS	37
CONCLUSIONS	41
FUTURE PLANS	43
ACKNOWLEDGEMENT	43
REFERENCES	44



OVERALL PROGRAM OBJECTIVES

The overall objective of this project is to provide an increased understanding of the secondary atomization process of Al/RP-1 slurry propellants. Specific objectives are as follows:

1. Develop an experimental system to measure the size and velocity of burning, 10-100 μm slurry droplets and to check for the presence of burning aluminum in these same droplets.
2. Use this experimental system to determine the ignition and secondary atomization characteristics of various slurry formulations.
3. From experimental data, develop an understanding of the role surfactants, gellants, and ultimate particle size play in the secondary atomization process.
4. Develop analytical models of droplet ignition and secondary atomization and apply these models in a 1-D rocket nozzle.

PROGRESS DURING REPORTING PERIOD

OVERVIEW

Recent work, presented in previous reports,¹⁻³ involved the development of experimental techniques that allow the study of small slurry droplets in the range of practical applications, e.g. 10-100 μm . Final shakedown of this experimental apparatus has been completed and attention has shifted to experimental measurements of particle size distribution at various axial locations above the burner, and the development of a model for the secondary atomization of Al/RP-1 slurry droplets. Since the size of the aluminum powder used in slurry fuels is of the order of several microns,^{4,5} and since the formation of a dense surface layer of particles is one mechanism for droplet disruption,⁶⁻¹⁰ the question arises of whether or not secondary atomization occurs when the parent droplet contains relatively few aluminum particles, rather than thousands. In prior work in our laboratories,¹¹⁻¹³ relatively large droplets (200-1200 μm) were studied, while in the present investigation, our focus is the secondary atomization of much smaller aluminum slurry droplets (20-100 μm).

THEORETICAL EFFORTS

DISRUPTIVE BURNING MODEL CONCEPTS

Recent studies by Lee and Law⁷ and Takahashi and coworkers^{9,10} present a simple theoretical framework for shell formation, an event which is considered to be an essential precursor for secondary atomization. This framework has been used to establish criteria for whether or not disruptive burning is possible for a particular slurry, and has been extended to include a specific mechanism for the process leading up to the droplet disruption. This model for the disruptive process will be refined over the next six months as more data become available.

Figure 1 schematically illustrates the sequence of events involved in the formation of a shell and its subsequent fragmentation. When exposed to a hot ambient environment, liquid vaporizes and the surface of the slurry droplet regresses following a "d²-law." The density of the solid particles at the surface increases until a rigid shell is formed by individual particles coming in contact with their neighbors (Fig. 1b). Experimental evidence suggests that the rigid surface layer is nominally three particle diameters thick with a solids volume fraction approximately equal to a cubic packing ($\theta_{s,p} = 0.524$).^{7,9} With the rigid shell, further vaporization of the liquid occurs at a constant external diameter. Additional growth of the shell thickness occurs, and conservation of mass requires that a void form somewhere in the interior of the slurry drop (Fig. 1c). The inner surface of the shell shrinks following a "d³-law."⁷ Takahashi and coworkers^{9,10} propose that pyrolysis of the surfactant concentrated in the surface layer causes the shell to become impermeable. This has the result that internal pressure builds up, since the vapor produced by heat conducted through the shell has no path of escape (Fig. 1d). Disruption occurs when the stresses in the shell are sufficiently high to meet some failure criteria.

RIGID SHELL FORMATION

To form a rigid shell requires that there are enough solid particles initially present in a slurry drop to form a hollow sphere with a specified thickness. The total number of particles in a droplet with an initially uniform solids volume fraction, $\theta_{s,o}$, is

$$N_{p,tot} = \theta_{s,o} (d_o / d_u)^3 \quad (1)$$

where d_o is the initial droplet diameter and d_u is the diameter of the individual solid particles.

SHELL FORMATION STAGES

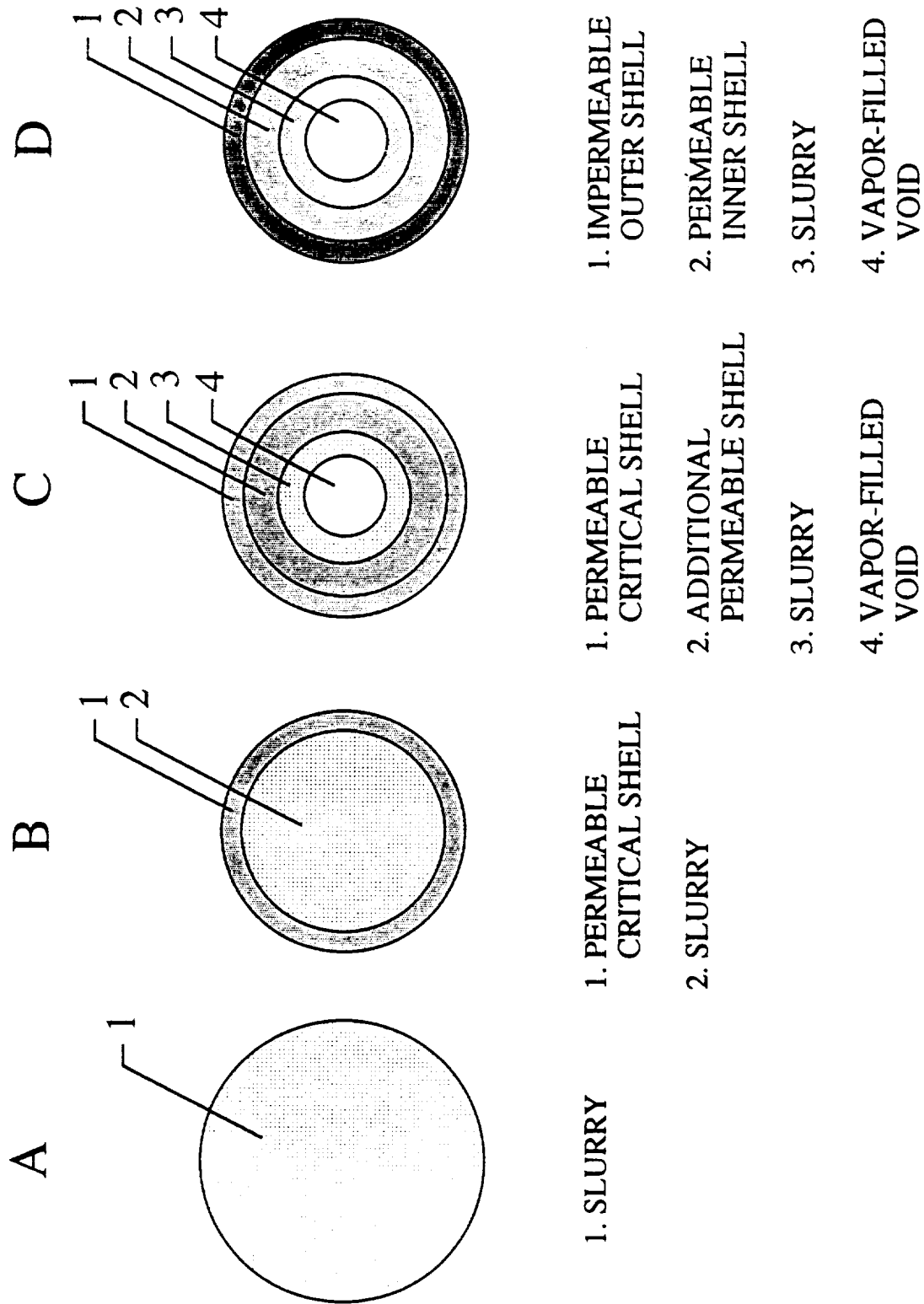


FIGURE 1. Schematic of critical shell formation, shell growth, vapor-void formation, and shell sealing.

The number of particles in the shell is a function of the assumed shell thickness and the diameter of the droplet when the shell becomes rigid, d_s . This is expressed

$$N_{p,s} = \theta_{s,p} \left[d_s^3 - (d_s - 2nd_U)^3 \right] / d_U^3 \quad (2)$$

where n is the dimensionless shell thickness ($n = \text{thickness}/d_U$), and $\theta_{s,p}$ is the solids volume fraction in the rigid shell. The remainder of the particles are in the liquid slurry core having the same solids volume fraction as the initial state, i.e.,

$$N_{p,tot} - N_{p,s} = \theta_{s,o} \pi (d_s - 2nd_U)^3 / 6. \quad (3)$$

The size of the droplet after enough liquid has evaporated to form the rigid shell can be obtained by substituting Eqs. (1) and (2) into Eq. (3) and solving for d_s . This involves a cubic equation that is easily solved numerically using Newton's method:

The limiting number of particles required to form a rigid shell nd_U thick can be obtained by recognizing that the smallest possible shell diameter is just twice the rigid shell thickness,

$$d_{s,lim} = 2nd_U, \quad (4)$$

and using this result, the minimum number of particles to form a shell can be expressed

$$N_{p,lim} = 8 \theta_{s,p} n^3. \quad (5)$$

The limiting initial droplet diameter can be obtained by setting the total number of particles [Eq. (1)] equal to the minimum number of particles required to form a shell [Eq. (5)] and solving for the initial diameter:

$$d_{o,lim} = 2nd_U \left(\theta_{s,p} / \theta_{s,o} \right)^{1/3}. \quad (6)$$

Equation (6) provides a criteria for determining whether or not a slurry drop of a certain size, d_o , has the possibility of undergoing secondary atomization, provided the constituent particle size and initial solids loading are known. Thus, for microexplosions to occur, we assume the following condition must be met:

$$d_o > d_{o,lim}. \quad (7)$$

To evaluate Eq. (6), we assume that $\theta_{s,p}$ is the value associated with cubic packing of spherical particles, and $\theta_{s,o}$ is determined by knowledge of the initial mass fraction of the solids, Y_s , as well as the solids and liquid densities, ρ_s and ρ_f , respectively:

$$\theta_{s,p} = 0.524, \quad (8a)$$

$$\theta_{s,o} = \frac{\rho_f Y_s}{\rho_f Y_s + \rho_s(1-Y_s)}. \quad (8b)$$

The preceding relationships [Eqs. (1)-(8)] were evaluated over a range of parameters that included those associated with the slurries employed in the experimental portion of this investigation. Figure 2 shows the minimum initial droplet size required to form a shell, expressed as a multiple of the constituent particle diameter, as a function of the aluminum mass loading. Curves are shown for assumed shell thicknesses of 2, 3 and 4 times the constituent particle diameter, d_u . Experimental evidence^{7,10} suggests that $n = 3$ is an appropriate value. As expected, the limiting initial diameter, $d_{o,lim}$, decreases as the aluminum mass fraction increases. Table 1 shows microexplosion limit parameters for the experimental slurries. Here we see that the minimum initial slurry droplet diameters were 34.7 μm and 38.1 μm .

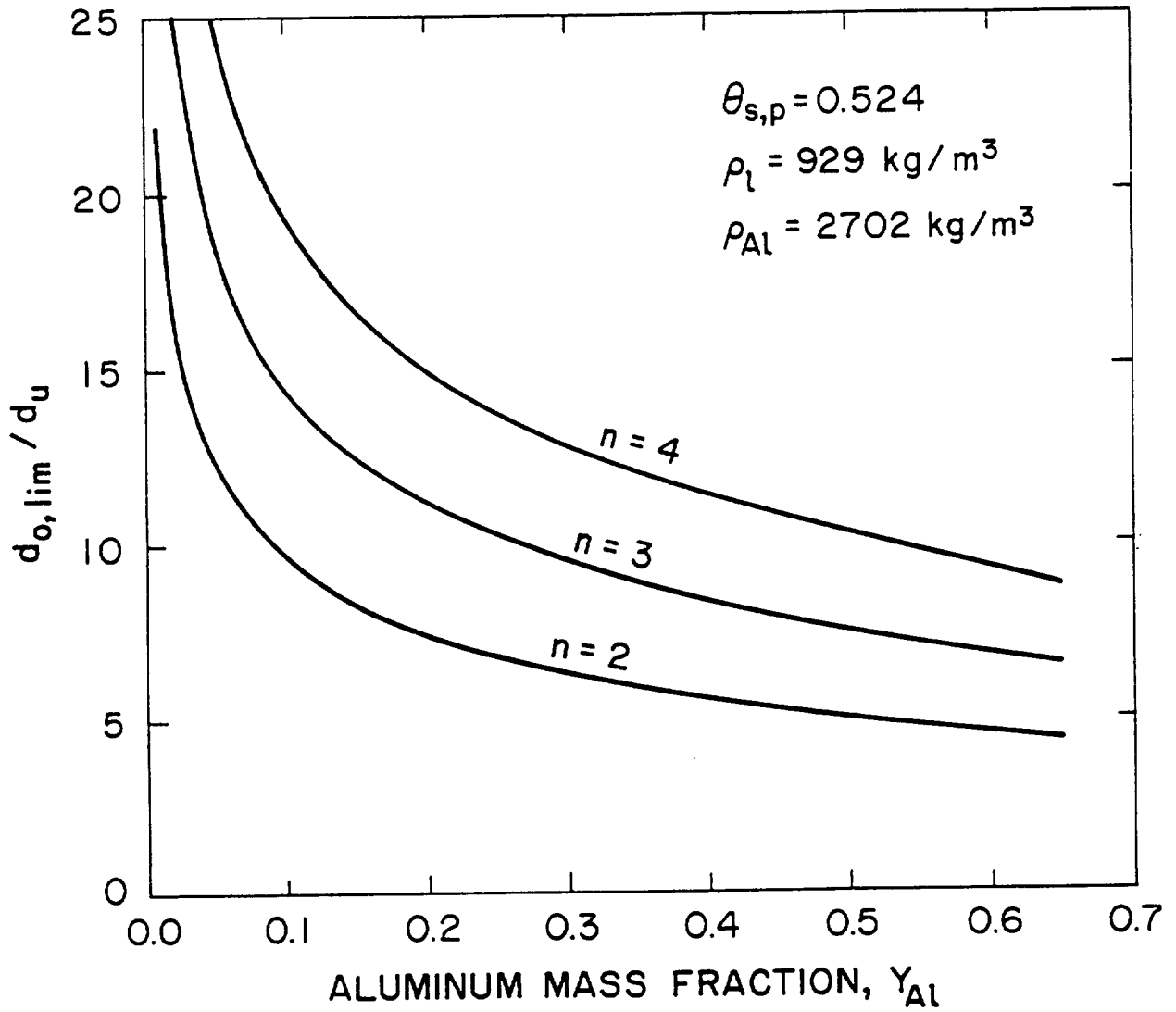


FIGURE 2. Dimensionless limiting initial diameter for the formation of a rigid shell as a function of aluminum mass fraction.

Table 1. Calculated Shell Limits^a
for Slurries Used in the Experiments

Slurry Designation	Aluminum Mass Fraction	d_u (mm)	$d_{o,lim}$ (mm)	d_s (mm)	$N_{p,lim}$
A	0.5	5	38.1	30	113
B	0.6	5	34.7	30	113

^a Calculated for $n = 3$, $\theta_{s,p} = 0.524$

The dependence of the rigid shell diameter on initial droplet diameter and constituent particle size is shown in Fig. 3. Also indicated in the figure are the total number of particles and the fraction of these that go into forming the rigid shell. For example, here we see that for an initial 100 μm droplet with 5 μm particles, the surface regresses to a diameter of about 82.6 μm , a decrease of 17.4 percent. A slightly greater percentage decrease in diameter (21.3%) is found for a 40 μm droplet. The limiting diameters and number of particles are indicated by the vertical lines at the left end of each curve. It is interesting to note that even for the largest droplet investigated ($d_o = 100 \mu\text{m}$), 78 to 90 percent of the total particles are required to form a shell for the aluminum slurries. In contrast, slurries of boron or carbon typically have much smaller constituent particles (d_u is typically between 0.1 and 1 μm), and hence, a much smaller fraction of the total particles is present in the shell. To illustrate the differences between aluminum and carbon slurries, calculated shell diameters and fractions of solids in the shell are shown as dashed lines on Fig. 3. The carbon slurry had the same mass loading as the aluminum slurry, but the particle size, d_u , was 0.3 μm . Here we see that very little diameter regression occurs and that the limiting initial diameter becomes quite small ($d_{o, \text{lim}} = 2.15 \mu\text{m}$). Based on the results shown in Fig. 3, one would expect carbon slurries to exhibit disruptive burning behavior down to much smaller initial droplet sizes, compared to aluminum slurries.

DISRUPTION

The rigid shell formation model developed by Lee and Law⁷ and described above has been extended to describe the processes leading up to droplet disruption. Figure 4 qualitatively illustrates the behavior of various parameters from the initial introduction of a slurry droplet into a high-temperature environment through disruption. This figure, together with Fig. 1, provides an overview of the simple disruption model developed below. Three important times are indicated on the ordinate of Fig. 4.: t_c , the

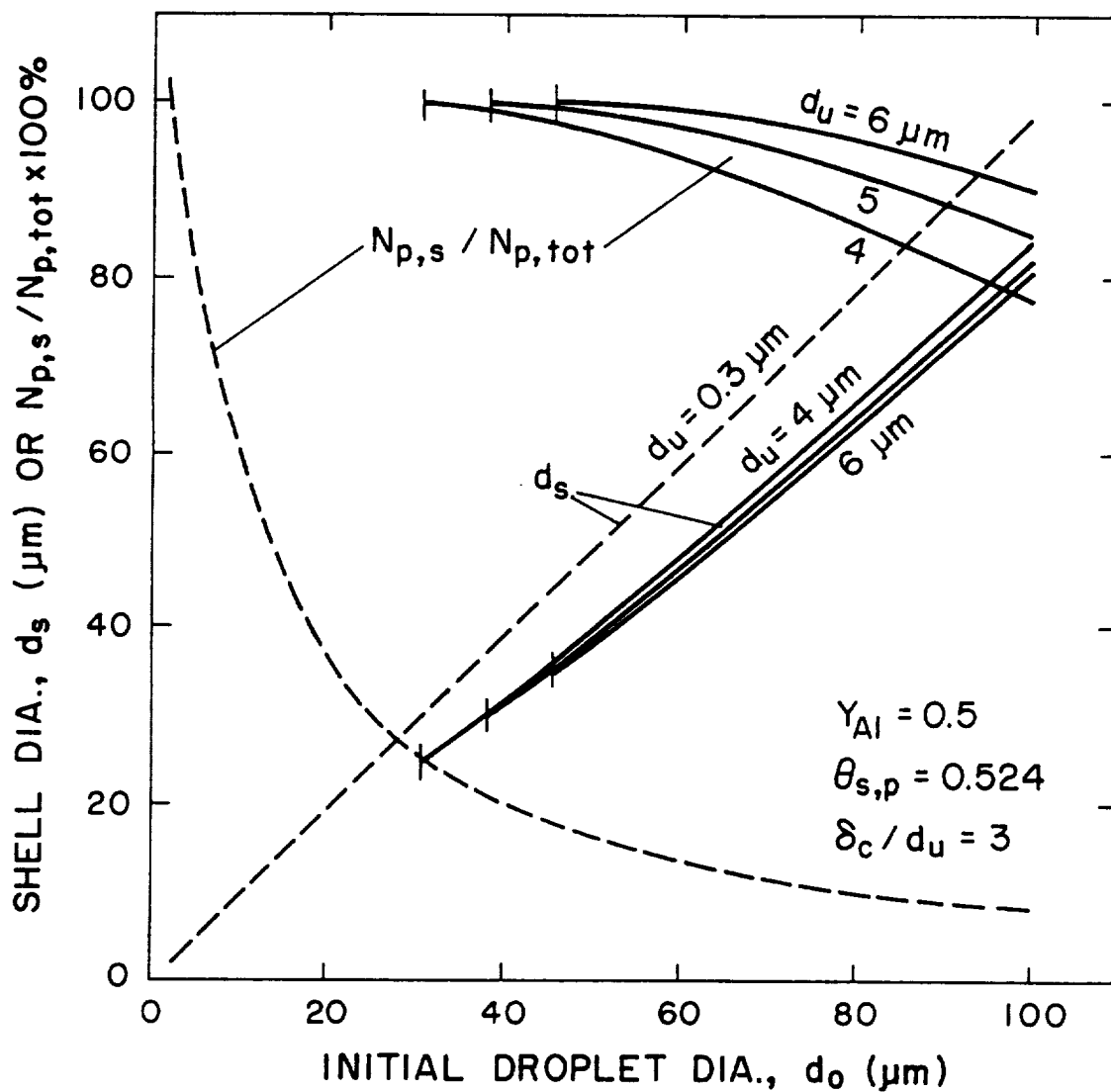
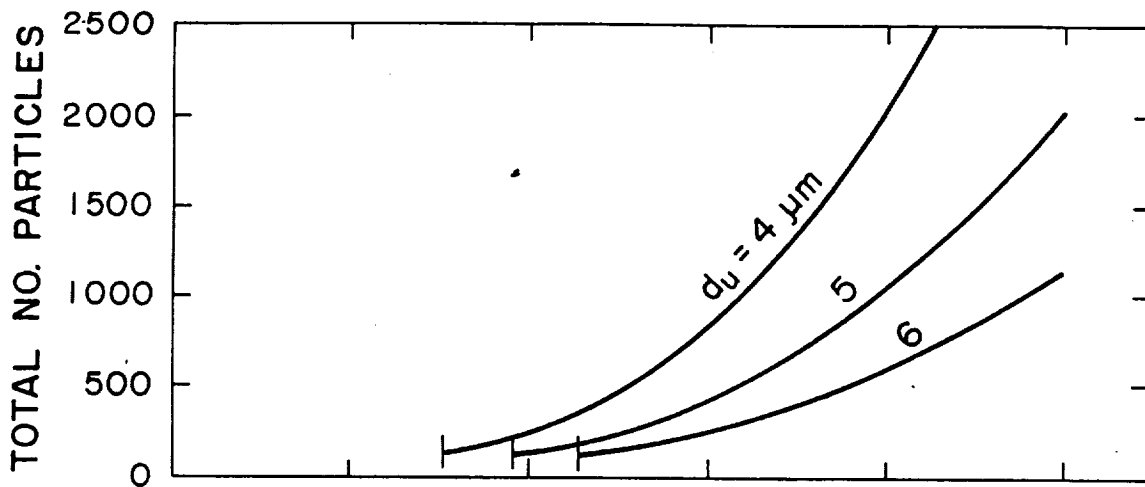


FIGURE 3. Shell diameter, the fraction of the total number of particles forming a critical shell and the total number of particles contained in the droplet as functions of initial droplet diameter.

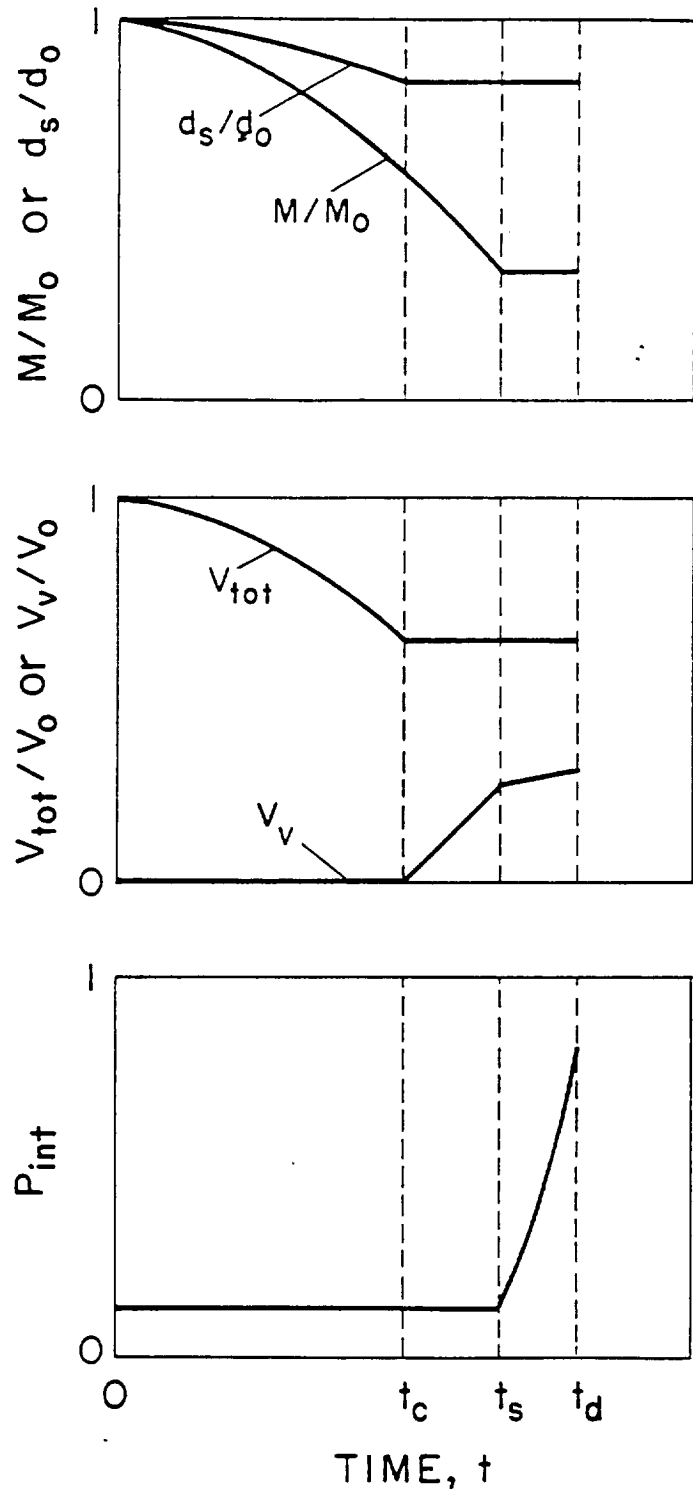


FIGURE 4. Schematic of processes leading up to disruption and the definition of the critical time to form a shell, t_c ; the time at which the shell seals, t_s ; and the time at which the shell ruptures, t_d .

critical time required to form a rigid shell; t_s , the time at which the shell becomes non-permeable; and t_d , the time at which the shell disrupts or breaks.

A conventional analysis¹⁴ of droplet vaporization, modified to account for the solids, is employed to calculate the diameter, mass, and volume of the droplet through the regressing-diameter stage up to the critical shell formation time, t_c . During this period,

$$\frac{d(d_s)}{dt} = -2\dot{m} / (\pi\rho_f d_s^2) \quad (9)$$

with the mass flux of evaporating fuel, \dot{m} , given by

$$\dot{m} = \frac{2\pi d_s k_g}{c_g} \ln \left[\frac{c_g (T_\infty - T_b) + h_{fV} + c_f (T_b - T_o)}{h_{fV} + c_f (T_b - T_o)} \right] \quad (10)$$

where k_g is the conductivity of the gas mixture; c_g and c_f are the specific heats of the gas and liquid, respectively; h_{fV} is the latent heat of vaporization; T_∞ is the ambient temperature; and T_o and T_b are the initial and boiling temperatures of the liquid fuel, respectively. In this particular approach, it is assumed that the surface temperature of the droplet is at the boiling point, which is a reasonable approximation.

Assuming constant properties, Eq. (9) can be integrated to yield

$$d_s^2(t) = d_o^2 - Kt \quad (11a)$$

where

$$K = \frac{8k_g}{\rho_f c_g} \ln(B+1) \quad (11b)$$

and

$$B = \frac{c_g (T_\infty - T_b)}{h_{fV} + c_f (T_b - T_o)} \quad (11c)$$

Since only the liquid evaporates, the mass of the droplet M , is simply determined by the volume change, i.e.,

$$M(t) = M_0 - \rho_l \pi (d_0^3 - d_s^3(t)) / 6. \quad (12)$$

The shell formation time can be determined by substituting the value of d_s when the shell is nd_u thick into Eq. (11a). This value of d_s is readily calculated knowing the solids volume fraction in the shell and in the bulk slurry using Eqs. (1)-(3), as discussed previously.

In the period between t_c and t_s , we assume that evaporation continues at a rate equal to that at the instant when the rigid shell forms, as has been done by other investigations.^{7,9,10} A more exact treatment would have to deal with the complex problem of flow through a porous medium that is not necessarily saturated with liquid. The mathematical description of such a flow is discussed in texts by Luikov.^{15,16} In fact, it is only through a detailed treatment that takes into account the local drying of the shell and subsequent pyrolysis of the high boiling point surfactants that the processes leading to the shell becoming impermeable can be fully understood. Such a treatment is beyond the scope of the present work, and thus, we treat the time interval $t_s - t_c$ as a parameter, which is varied to see its effect.

During the period between t_c and t_s , the rigid shell grows in thickness and a vapor void forms. With the evaporation rate given Eq. (10), the shell interior equivalent diameter, d_p , and the vapor void cavity equivalent diameter, d_v , can be calculated by integrating simple mass and volume balances. The resulting expressions are:⁷

$$d_p^3 = (d_{s,c} - 2nd_U)^3 - \frac{3\theta_{s,o} d_{s,c} K(t_s - t_c)}{2(\theta_{s,p} - \theta_{s,o})} \quad (13)$$

$$d_v^3 = 3d_{s,c} K(t_s - t_c) / 2 \quad (14)$$

where the rigid shell is assumed to be wet with the liquid fuel. The volume of the vapor is directly determined from Eq. (14) as

$$V_v = \pi d_v^3 / 6, \quad (15)$$

while the volume of the liquid is the total volume minus the vapor and solids volumes:

$$V_l = \pi (d_{s,c}^3 - \theta_{s,o} d_o^3 - d_v^3) / 6. \quad (16)$$

Equations (15) and (16) provide two of the several initial conditions necessary to calculate the internal pressure history after the shell seals.

Pressure Build-up

To gain some initial insights into the pressure build-up phenomena, the solids-liquid-vapor system is treated as a single thermal lump, with the liquid and vapor existing as a saturated mixture of a single component fuel. Furthermore, we assume that the outer shell diameter, $d_{s,c}$, is fixed; hence, the total volume does not change as the pressure builds up. For purposes of illustration, the properties of JP-10 are used. Conservation of energy for the lumped system is expressed:

$$q_c = \frac{dU}{dt} = \frac{d}{dt} (M_v u_v + M_l u_l + M_s u_s) \quad (17)$$

where q_c is the energy convected to the ambient hot gas to the shell surface, U is the total system internal energy, and u_j is the specific internal energy of the j phase.

Introducing the quality, x , of a wet mixture, defined as the mass fraction of the vapor in the mixture, the liquid-vapor mixture internal energy is

$$U_m = M_v u_v + M_f u_f = M_m (u_f + x u_{fv}) \quad (18)$$

where u_{fv} is the internal energy of vaporization and M_m is the liquid-vapor mixture mass. Treating the vapor phase as a pseudo-ideal gas with a constant compressibility factor, z , u_{fv} can be related to the enthalpy of vaporization, h_{fv} , as follows:

$$u_{fv} = h_{fv} - P \left(\frac{zRT}{P} - v_f \right) \quad (19)$$

With a rigid impermeable shell, the mass and the volume of the liquid-vapor system are constant, hence

$$v = v_f + x v_{fv} = \text{constant} \quad (20)$$

Solving Eq. (20) for x and substituting the result into Eq. (18), together with the substitution of Eq. (19), yields

$$U_m = M_m \left\{ c_{pf} T + \frac{v - v_f}{\frac{zRT}{P} + v_f} \left[h_{fv} - P \left(\frac{zRT}{P} - v_f \right) \right] \right\} \quad (21)$$

where we assume $u_f = c_{pf} T$.

The enthalpy of vaporization as a function of temperature can be approximated in terms of the critical temperature, T_c , and a reference temperature, T_o , at which the enthalpy of vaporization is known:¹⁷

$$h_{fv} = h_{fv,o} \left[\frac{(1 - T / T_c)}{(1 - T_o / T_c)} \right]^{0.375} \quad (22)$$

Since we are dealing with a wet mixture, the pressure and temperature are not independent properties. Thus we employ the Clausius-Clapeyron equation to relate the saturation temperature and pressure, i.e.

$$P = A \exp(-B / T) \quad (23)$$

For JP-10, A has a value of $3.069 \cdot 10^9$ Pascals, and B has a value of 4704.2 Kelvins.¹⁸

Substituting Eq. (22) and (23) into Eq. (18) and differentiating with respect to time yields

$$\frac{dU_m}{dt} = M_m(\alpha_1 + \alpha_2 + \alpha_3) \frac{dT}{dt} \quad (24a)$$

where

$$\alpha_1 = c_{pf}, \quad (24b)$$

$$\alpha_2 = \frac{(v - v_f) \left[\left(\frac{zRT}{P} - v_f \right) \beta - h_{fv} \frac{zR}{P} (1 - B/T) \right]}{\left(\frac{zRT}{P} - v_f \right)^2}, \quad (24c)$$

$$\alpha_3 = (v - v_f) A B \exp(-B/T) / T^2, \quad (24d)$$

and

$$\beta = \frac{-0.375 h_{fv,0}}{(T_c - T_0)^{0.375} (T_c - T)^{0.625}}. \quad (24e)$$

The liquid specific volume v_f has been assumed constant.

Substituting Eq. (24) into the energy balance (Eq. 17) for the solids-liquid-vapor system and solving for the temperature derivative yields

$$\frac{dT}{dt} = \frac{q_c}{\left[M_m(\alpha_1 + \alpha_2 + \alpha_3) + M_s c_{ps} \right]} \quad (25)$$

where it is assumed that $u_s = c_{ps}T$.

The integration of Eq. (25) provides the temperature history of the slurry droplet after the shell seals, and via the Clausius-Clapeyron relation (Eq. 23), the pressure history is determined. The instantaneous convective heat transfer rate is given by

$$q_c = h\pi d_{s,c}^2 (T_\infty - T) \quad (26)$$

where h is the heat transfer coefficient which is determined by the Nusselt number, i.e.,

$$h = k_g \text{Nu}/d \quad (27)$$

Brittle Shell Failure

Consistent with a fixed volume during pressure build-up, we assume that the microexplosion event is triggered by the failure of a brittle shell. For a thin shell, the internal stress level is readily calculated knowing the pressure difference across the shell:

$$\sigma = \frac{\Delta P r}{2\delta} \quad (28)$$

where r is the mean shell radius and δ is the shell thickness at the instant the shell seals.

Model Results

Figures 5a, b, and c illustrate the shell thickness, δ ; the percentage of the initial liquid fuel remaining; and the stress build-up in the shell as functions of the time after the critical shell thickness is achieved for initial droplet sizes of 50, 100, and 200 μm , respectively. Thus, at time equals zero, the shell thickness, δ , is $3d_u$ or 15 μm . For the 50 μm drop-size, very little slurry remains after the critical shell is formed, so δ grows only slightly ($\sim 6\%$) as the remaining solids are added to the shell as the liquid evaporates. In contrast, the shell on the 200 μm drop has the potential to increase up to 83% in thickness, if evaporation continues without the shell becoming impermeable and sealing the remaining fuel inside the shell.

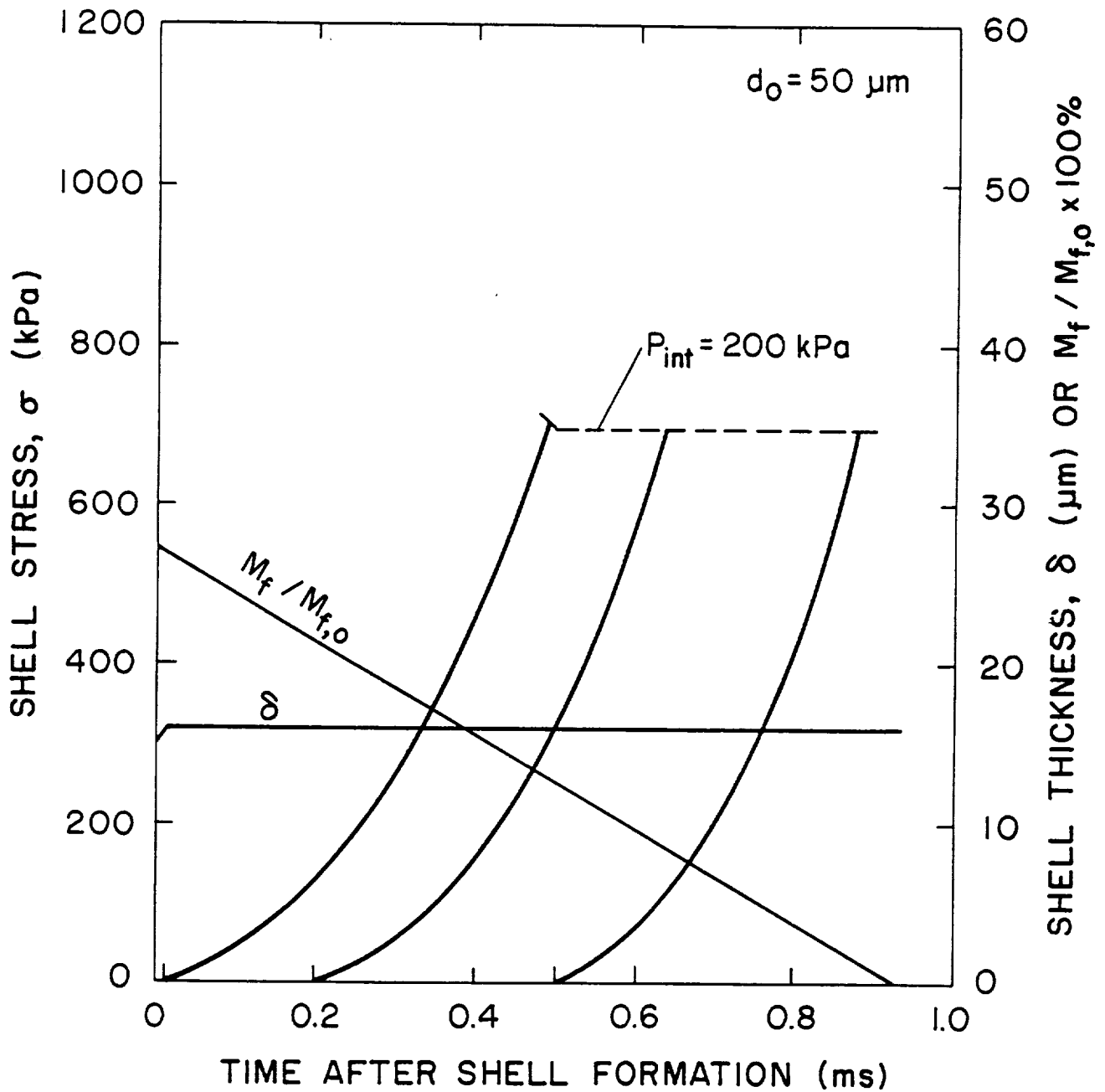


FIGURE 5a. 60 wt% aluminum slurry droplet ($d_0=50 \mu\text{m}$) shell stress, liquid fuel mass fraction and shell thickness as functions of time assuming various shell sealing time intervals ($d_{\text{ult}}= 5 \mu\text{m}$).

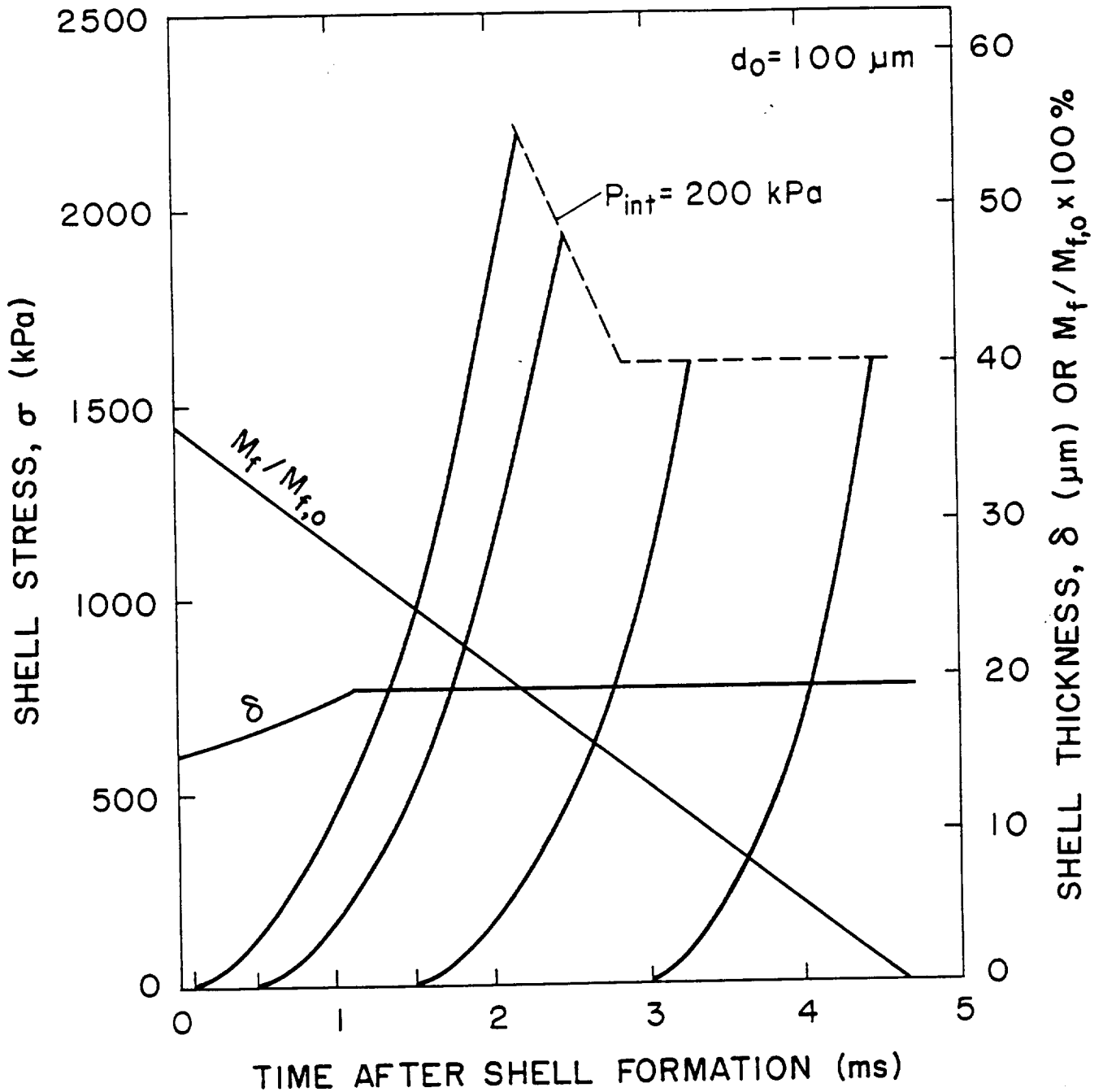


FIGURE 5b. 60 wt% aluminum slurry droplet ($d_0=100 \mu\text{m}$) shell stress, liquid fuel mass fraction and shell thickness as functions of time assuming various shell sealing time intervals ($d_{\text{ult}}=5 \mu\text{m}$).

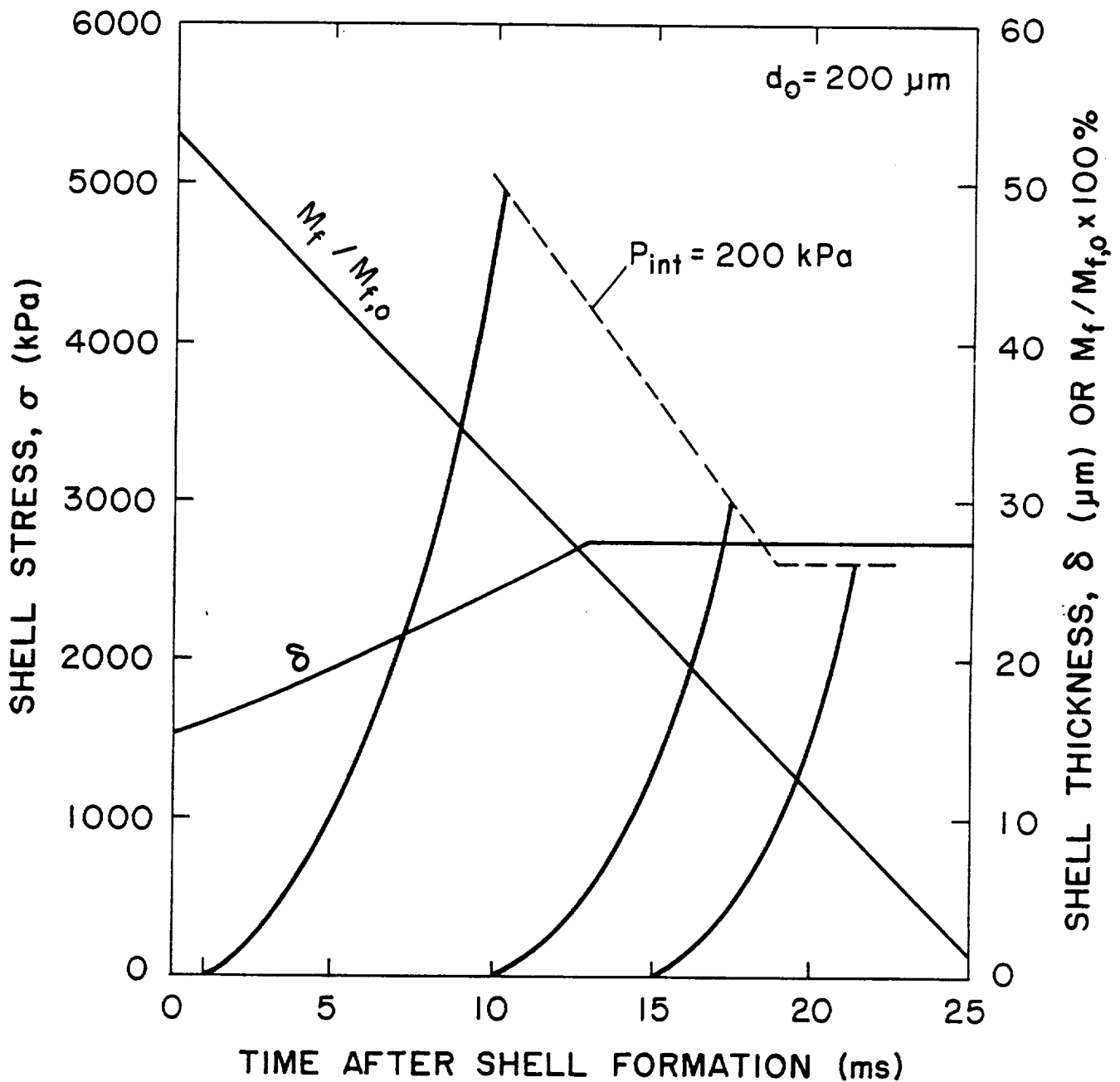


FIGURE 5c. 60 wt% aluminum slurry droplet ($d_0=200 \mu\text{m}$) shell stress, liquid fuel mass fraction and shell thickness as functions of time assuming various shell sealing time intervals ($d_{\text{ult}}=5 \mu\text{m}$).

The shell stress, σ , is shown as a family of three or four lines, with each line corresponding to a different assumed shell sealing time. For example, in Fig. 5a, the stress build-up is shown for assumed shell sealing times of 0.01, 0.2, and 0.5 ms. At the instant the shell seals, the mass fraction of the JP-10 becomes fixed and the pressure, and consequently the stress, then begins to increase. For the 50 μm droplet case, we see that the stress increases at essentially the same rate, regardless of the shell sealing time, as a consequence of the shell thickness being identical for each of the three histories shown. For the 200 μm drop, the stress increases more rapidly for the earlier sealing times since the shells are thinner and have not yet reached their maximum thickness. We note also that the stress levels increase with the initial droplet diameter. This is a consequence of the larger mean shell radius, since the pressure levels for all cases ranged from an initial atmospheric value to 200 kPa.

The above results imply that the larger droplets are more likely to fragment than the smaller droplets because of the higher stresses; and furthermore, the consequence of the larger drop's fragmenting is likely to be much more beneficial since the potential for spewing out raw slurry, rather than just producing shell fragments, is greater. In fact, for the 50 μm droplet, only shell fragments can be produced if sealing occurs later than 0.01 ms after the critical rigid shell is formed.

EXPERIMENTAL EFFORTS

A schematic of the overall experimental apparatus, discussed in previous reports,¹⁻³ is presented in Fig. 6. Significant progress has been made in the detection of burning aluminum and in the handling/atomization of slurries. The 90° optics of the sizing/velocity system have been modified to ensure that the signal validation and aluminum combustion detection probe volumes are the same. However, these

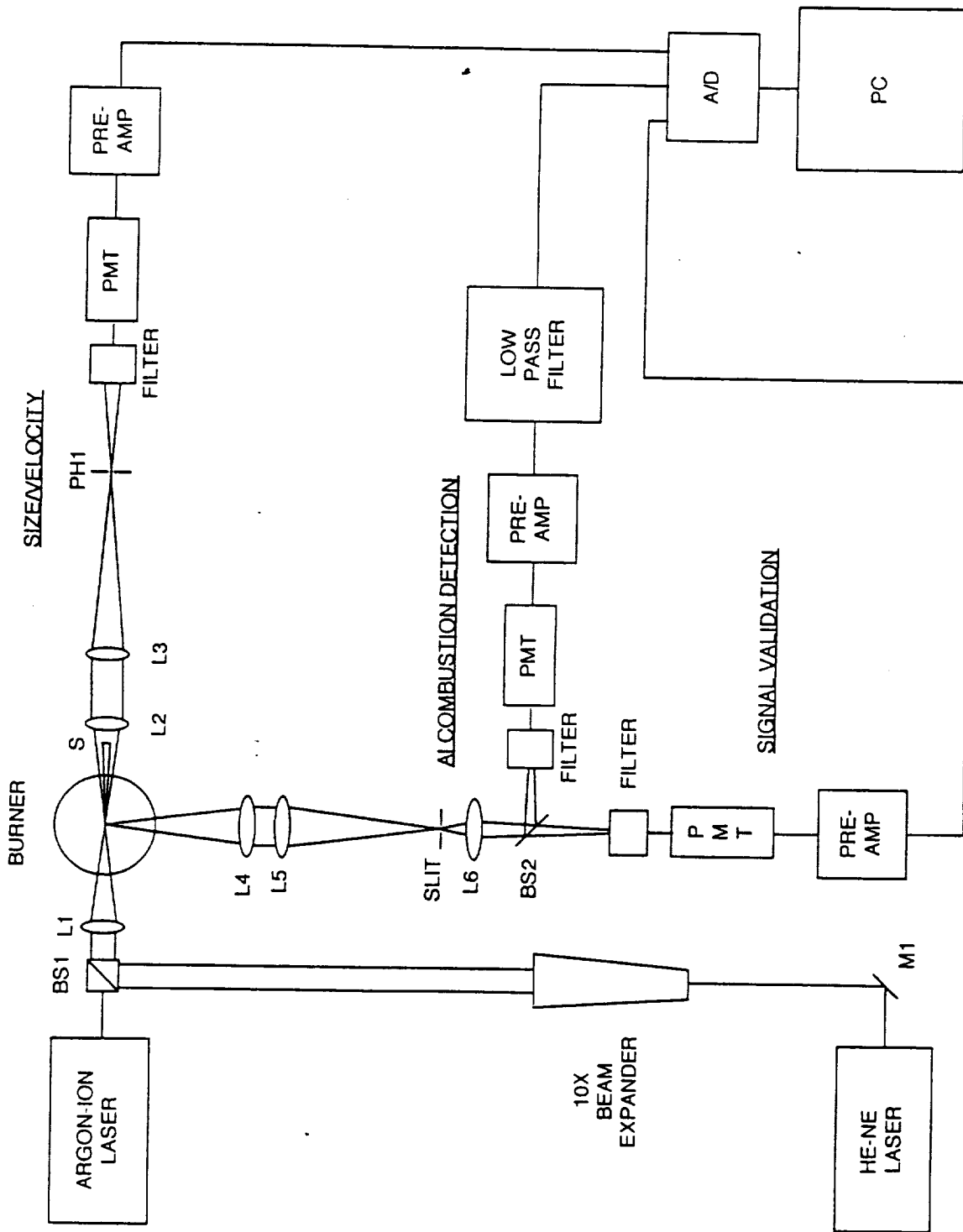


FIGURE 6. Schematic of experimental apparatus.

changes do not affect the basic operating principles of the system, described in an earlier report.¹

ALUMINUM COMBUSTION DETECTION

The aluminum combustion detection system and complications encountered in the detection of burning aluminum have been discussed in a previous report.³ As previously mentioned, the detection of burning aluminum is complicated by the presence of broadband radiation from both Al_2O_3 and burning hydrocarbons, neither of which marks the aluminum combustion process. Spectral emission data^{19,20} show two strong spectral line emissions from vapor-phase aluminum in the 395 nm wavelength region, as seen in Fig. 7. These spectral lines provide a valid indication of burning aluminum since vapor-phase aluminum only exists during combustion. Based on these considerations, an aluminum combustion detection system, consisting of a 395 nm bandpass filter and a photomultiplier tube (PMT), was incorporated in the 90° scatter channel. Due to the high gain levels employed for this PMT, it was necessary to pass the signal through a low-pass filter to remove high frequency noise from the signal prior to processing. To determine the correct cut-off frequency, a variable filter (Ithaco Model 4302) was used in shakedown tests involving burning aluminum. A cut-off frequency of 10 kHz was found to provide the best ratio of signal resolution and noise filtering. Following this testing process, a dual pole 10 kHz low pass filter was constructed and installed.

Peak blackbody (broadband) emission from molten aluminum, solid or molten alumina, and soot associated with burning hydrocarbons typically occurs at wavelengths longer than 395 nm, as can be seen in Fig. 8. These broadband emissions generate a low-level background noise on the combustion detection signal. It is therefore necessary to determine a minimum threshold signal level to discriminate

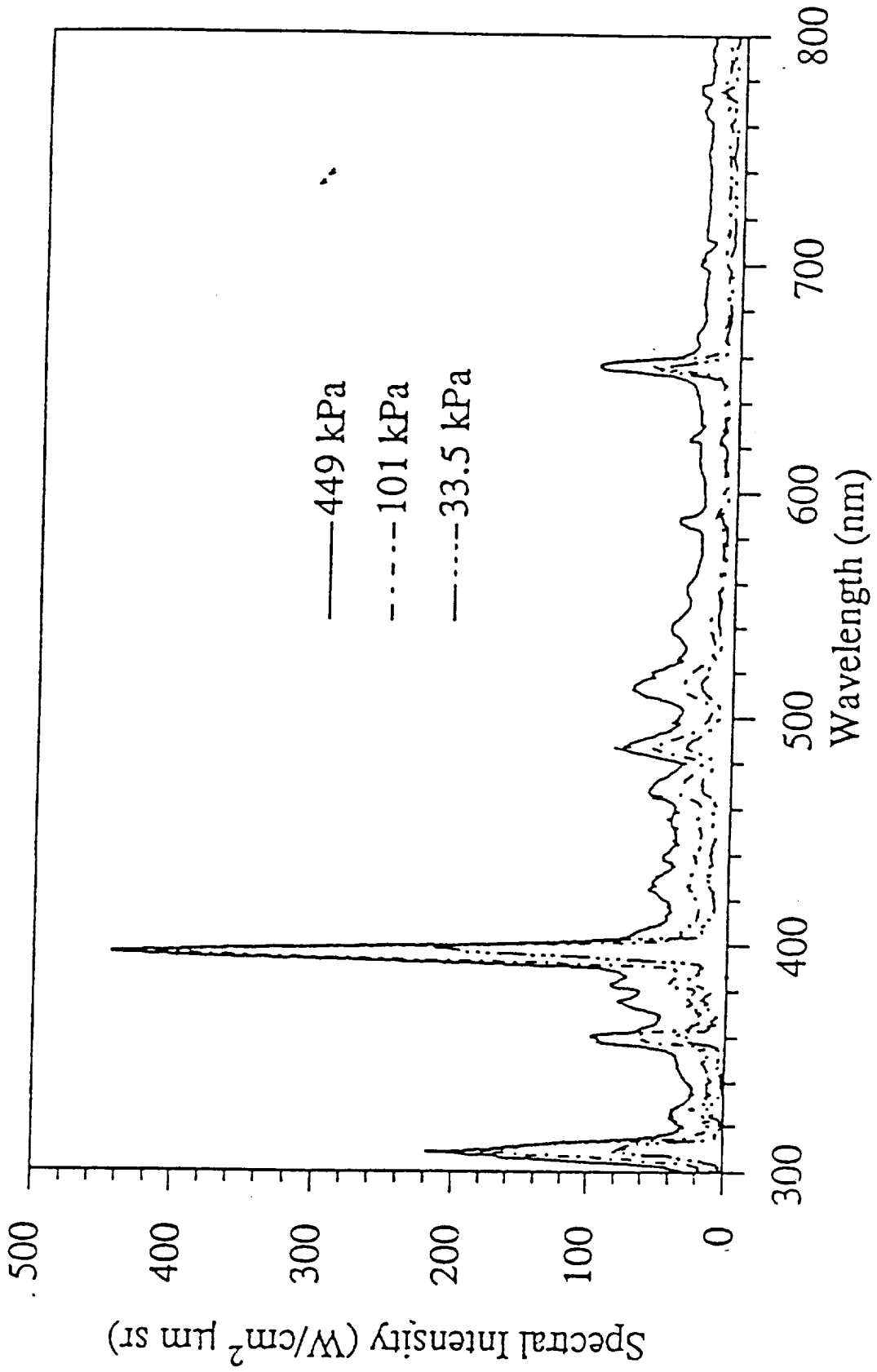


FIGURE 7. Spectral intensity versus wavelength for reacting aluminum
 From: Jones, M.R. and Brewster M.Q., "Radiant Emission from the Aluminum-Water Reaction",
 Journal of Quantitative Spectroscopy and Radiative Transfer

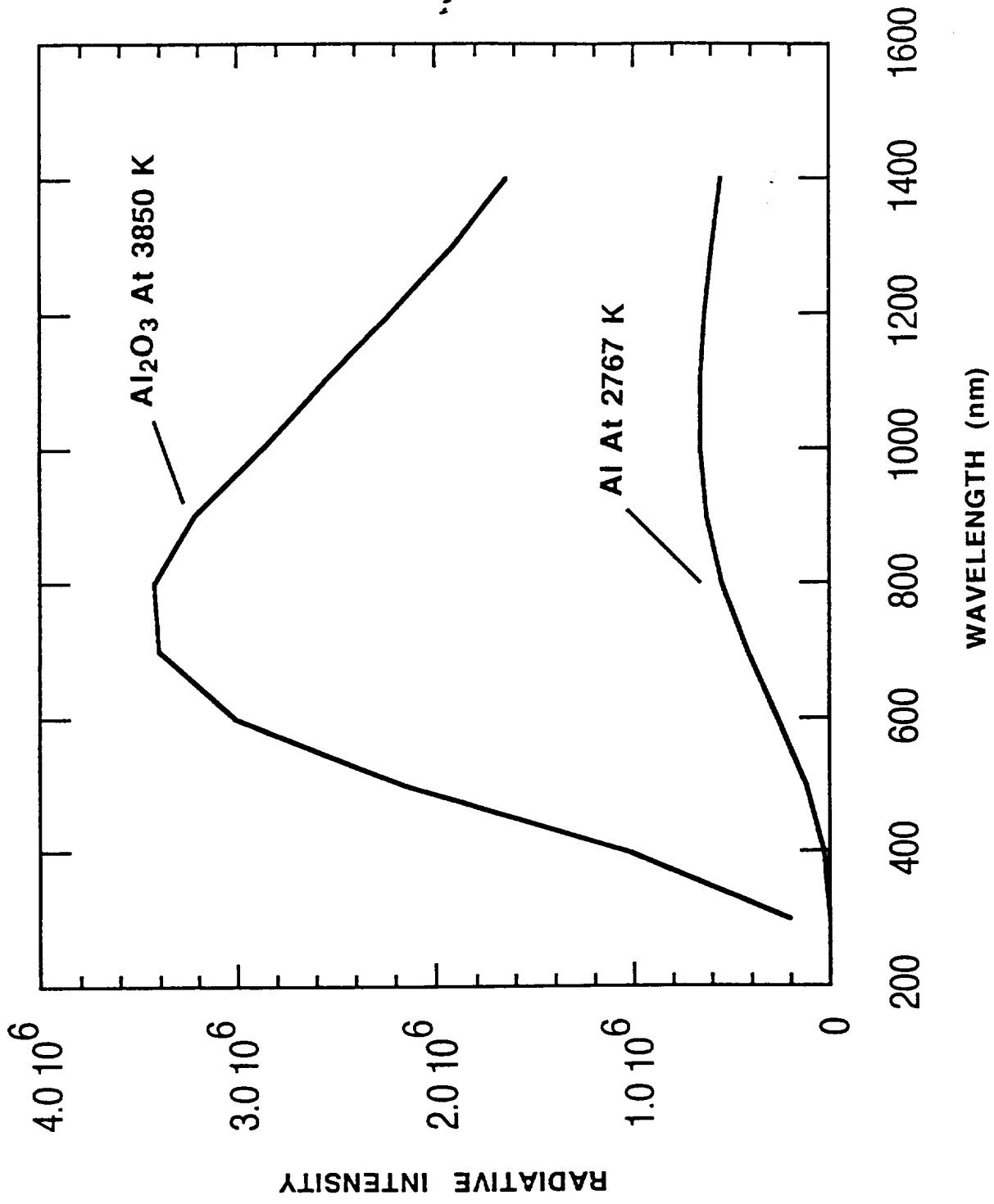


FIGURE 8. Blackbody radiative intensity distributions for boiling aluminum and aluminum oxide.

between valid aluminum combustion and this background radiation. Figure 9a is a scattergram of the combustion channel voltage versus droplet diameter for burning JP-10 droplets. As can be seen, the maximum voltages recorded are nominally less than 2 volts for all droplet diameters. This voltage level is slightly higher than the 0.8 volt maximum noise level measured with no flame, most likely due to broadband emissions from soot. Figure 9b is a similar scattergram for a 60 wt% aluminum slurry. In contrast, for this case, there are many particles with ignition signals much higher than 2 volts. The majority of these signals are associated with particles less than 15 μm in diameter, indicating that the smaller aluminum agglomerates are burning out. From these data, a 2 volt threshold was chosen as the criterion for aluminum combustion, since this was the highest signal level observed in the absence of aluminum combustion.

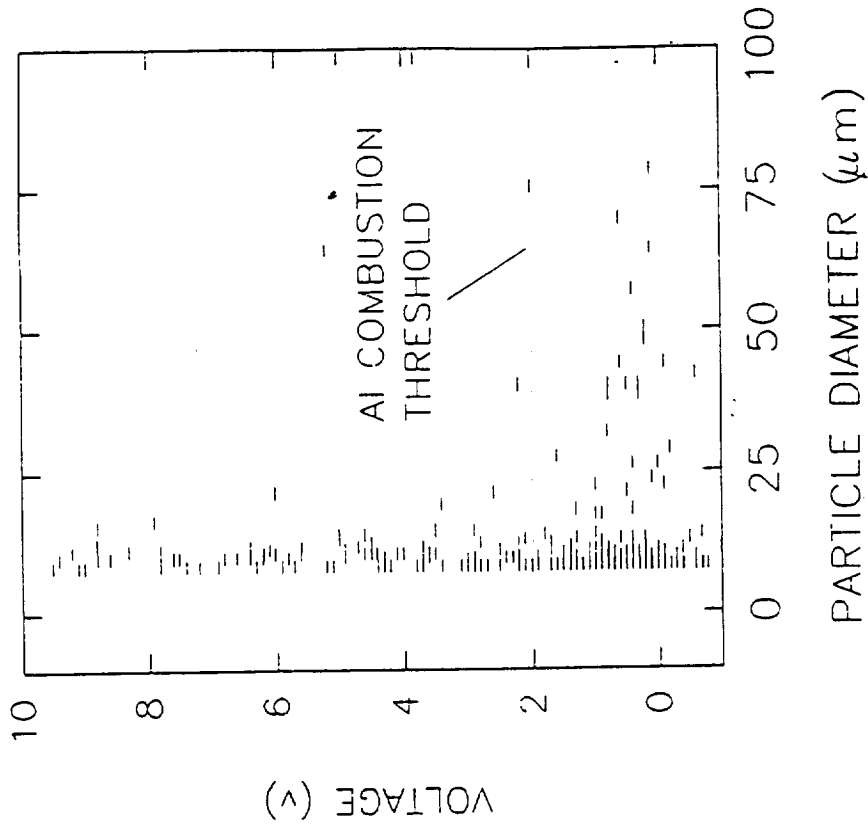
SLURRY ATOMIZATION

Long-term steady-state atomization of the slurries is critical in obtaining valid and repeatable experimental results. For this reason, extensive tests of the atomizing system were conducted, and atomizer operating procedures were adjusted to improve this steady-state operation. It was found that performance degraded slightly over time due to slurry clogging the atomizing nozzle and that changing feed syringes had the potential to flood the nozzle. Increasing the atomizing gas flow rate improved the long-term stability of the system, and allowing the atomizing gas to flow during syringe changes alleviated the flooding problem.

Using the above mentioned procedures, the system was operated over a period of two hours using a 60 wt% aluminum slurry[†] with droplet size distributions collected

[†] 60 wt% aluminum slurry- Sun Refining, Inc. Blend # 942438

AI/RP-1 SLURRY



JP-10

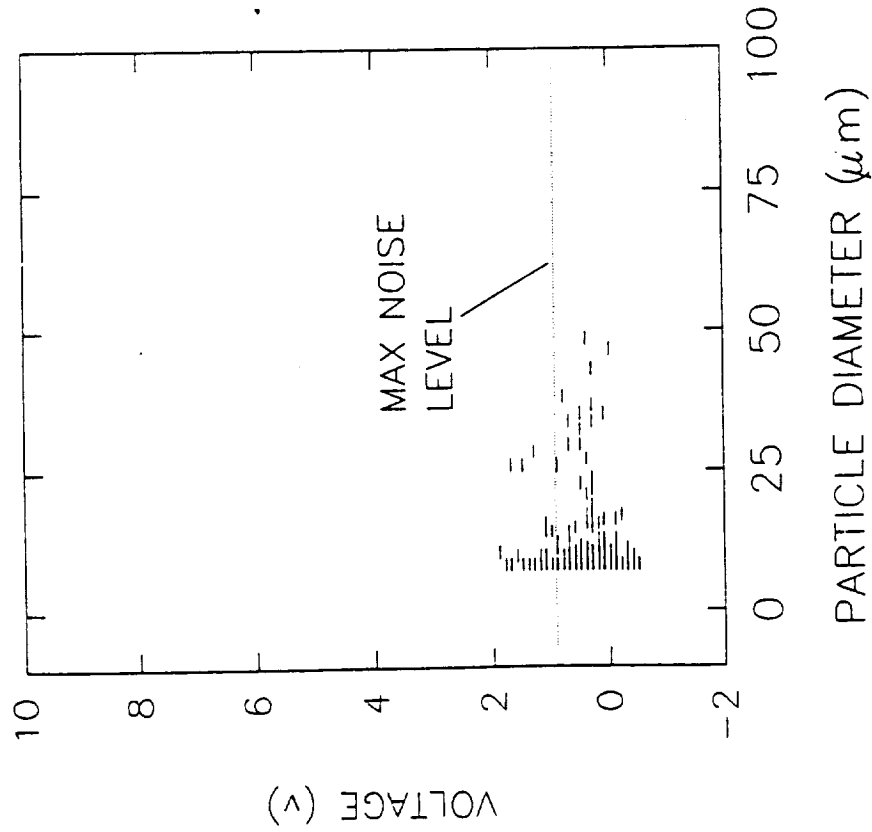


FIGURE 9a,b. Aluminum combustion signal level versus droplet diameter for JP-10 and 60 wt% aluminum slurry particles respectively (Sun Formulation 942438).

at a fixed point above the burner every 20 minutes. These distributions were then compared, and no variations were found. A count of visible microexplosions versus time was also conducted. No significant variation in microexplosion frequency was encountered. These tests indicate that the atomizer is providing long-term steady-state atomization.

COMBUSTION AND IGNITION TESTS

Test Objectives

Preliminary comparisons of disruption frequency and intensity between a carbon slurry, containing small ultimate particles ($d_{ult} = 0.8 \mu\text{m}$), and an aluminum slurry, containing larger ultimate particles ($d_{ult} = 4 \mu\text{m}$), were made to verify the predicted effects of ultimate particle diameter on the droplet disruption process. Aluminum slurry droplet combustion tests were performed in which particle size and velocity distributions were measured to experimentally verify the calculated minimum initial droplet diameter capable of undergoing disruption. Simultaneous detection of burning aluminum particles provided experimental aluminum agglomerate ignition times for small diameter agglomerates, which were then compared with analytical results.

Carbon Slurries

According to shell formation theory, smaller ultimate particles should allow smaller initial diameter droplets to form rigid shells. To test this hypothesis, some effort was invested in the study of the atomization and combustion of a carbon slurry.^{††} Atomization tests indicate that the carbon slurry has a much greater tendency to clog the atomizing nozzle, making long-term steady-state operation more difficult.

^{††} SF₂ carbon slurry provided by NASA Lewis

However, recent refinements in atomizer operation methods should alleviate this problem. Qualitative observations of droplet combustion indicate that the carbon slurry appears to be more active than a 60 wt% aluminum slurry in terms of visible microexplosion frequency. However, the intensity of the carbon slurry microexplosions appear to be weaker than those observed in the aluminum slurries. This work will be extended to provide more quantitative measurements of carbon slurry disruption.

Aluminum Slurries

Test Conditions - Methane was the burner fuel and the oxidizing gas was a N_2/O_2 mixture. The burner test condition is presented in Table 2. At this high-temperature condition, size, velocity, and aluminum combustion data for 60 wt% slurry droplets, were collected at several axial locations. The threshold voltage level on the signal validation channel, which triggers the acquisition process, was increased for this experiment. Due to the Gaussian intensity distribution of the laser beam, and the fact that a small particle scatters less light than a large particle for a given incident intensity, the effective sample volume for small particles will be less than that for larger ones, resulting in an underrepresentation of the small particle population.^{3,21} In order to obtain the true size distribution in a data set, it is necessary to apply a probability distribution function (PDF) to the data.^{3,22} The atomization system generates a much greater number of particles in the 10-20 μm size range than at larger sizes. This distribution results in data sets containing many small particles and few in the 20-50 μm range, which is of particular interest. Therefore, a higher trigger level was used to intentionally increase the data collection bias towards the larger particles, allowing shorter collection times than would otherwise be necessary.

Table 2. Burner Test Conditions

Equivalence Ratio	O ₂ Mole Fraction	Temperature (K)	Post-Flame O ₂ Mole Fraction
0.6	0.56	2650	0.18

Data were collected at each axial location for a period of 20 minutes. Comparison with data sets collected over much longer time periods indicates that 20 minutes is sufficient to obtain qualitatively repeatable size distributions.

Results - Size and ignition data for the 60 wt% slurry at $x = 5, 10,$ and 15 mm are presented in Fig. 10. Figure 10a and 10b show respective size distributions for a cold and a hot flow, 5 mm above the burner. Figure 11 is a typical histogram of particle number versus velocity for the data from Fig. 10a-d. The average particle velocity was calculated to be approximately 7 m/s, ranging from 2-10 m/s. The few high-velocity signals are most likely due to noise or insufficient signal resolution at the low end of detectability.

The most obvious feature of Fig. 10 is the apparent bimodal distribution of particle sizes. This distribution may be due to the atomizing system characteristics or might be an artifact of not applying a correction for trigger bias. In either case, the data are valid for comparisons between the same size classes at different axial locations since the same correction applies at all axial locations. However, only qualitative comparisons of overall particle distributions are possible without correction for trigger bias.

Before comparisons between experimental and theoretical results can be made, it is necessary to determine the axial location at which droplet combustion begins. Combustion is unlikely to start at the burner surface since the droplets must first pass through the core of a diffusion flame above the central tube. The core of this flame contains no oxygen and should be relatively cool, preventing droplet ignition and combustion, and resulting in little evaporation. In contrast, the flame front is hot, and oxygen is present, allowing ignition and combustion of the droplets. Although the

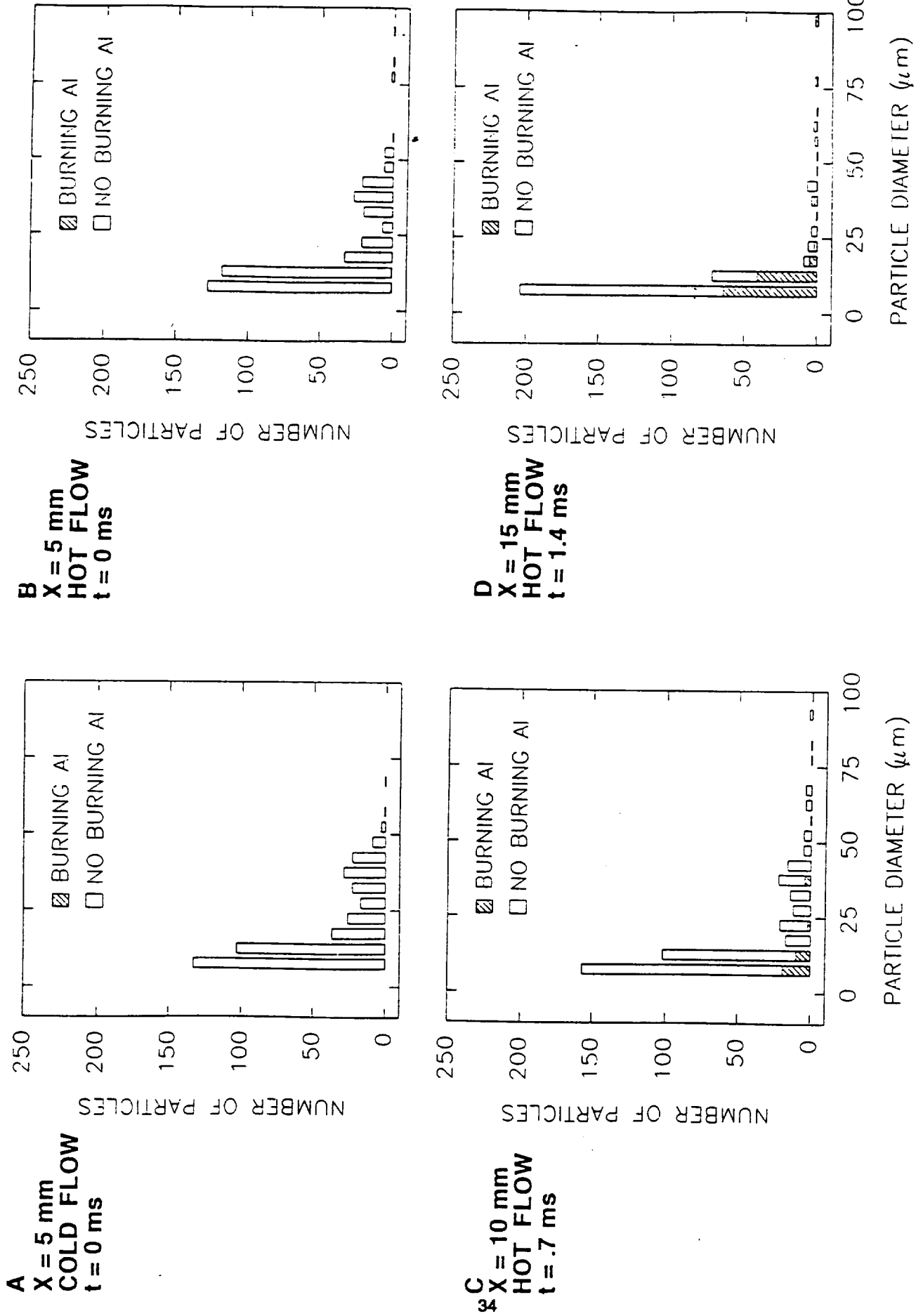


FIGURE 10a-d. 60 wt% aluminum slurry particle size distributions at several locations above the burner surface. (Sun Inc. Formulation 942438)

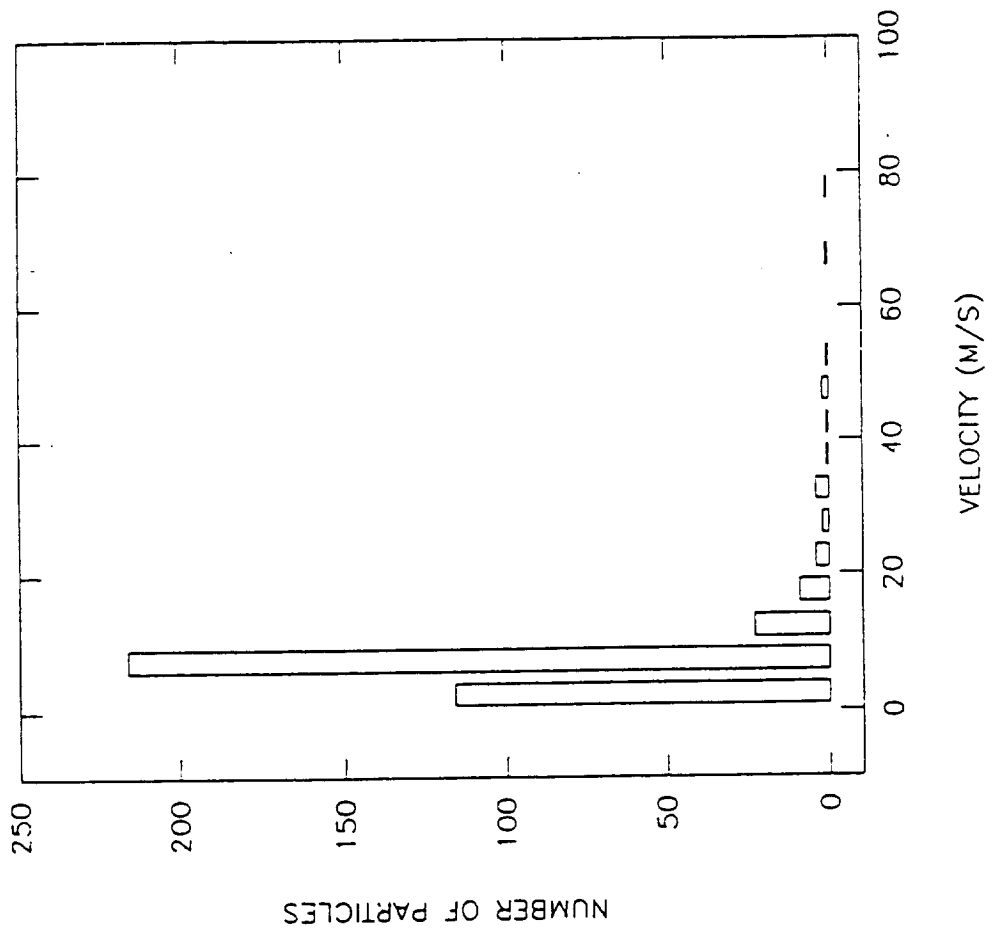


FIGURE 11. Typical velocity histogram for 60 wt% aluminum slurry particles.

height of this flame is not clearly defined, the tip is between 3 and 7 mm above the burner face as evidenced by the height of the surrounding burner flames.

The idea of droplet evaporation beginning some distance above the burner surface is further supported by the data collected at $x=5$ mm. Examining Figs. 10a and 10b, we see that there are no major differences between the size distributions of the hot and cold flows, indicating that the amount of droplet evaporation within 5 mm of the burner surface is small for this particular test condition. This fact, coupled with the lack of aluminum combustion, represented by the unshaded portions of the histograms, indicates that little combustion activity is occurring over the first 5 mm.

The data in Fig. 10c ($x = 10$ mm) show a slight shift toward smaller particles in comparison to the $x=5$ mm position. This is particularly evident in the 5-15 μm range. Aluminum combustion is first seen to appear in this same size range, as would be expected, since small slurry particles lose their hydrocarbon liquid component sooner than large particles. The faster liquid burnout results in shorter agglomerate ignition times for the small particles.

Figure 10d ($x = 15$ mm) shows a sharp decrease in the number of particles in the 20-40 μm range and a substantial increase in the number of particles in the 10-15 μm region. These changes do not result from simple liquid evaporation, since calculations indicate that a slurry droplet with an initial diameter of only 28 μm would still form a 20 μm diameter agglomerate. Hence, agglomerate formation from the 20-40 μm droplets should give rise to an increase in particle number in the 20-30 μm range rather than the 10-15 μm range. These facts lead to the conclusion that secondary atomization of particles in the 20-40 μm range is occurring between the 10 and 15 mm axial locations. This conclusion is also consistent with visual observations

of sudden bursts of glowing particles in this same region and higher in the flame, with very few below 10 mm.

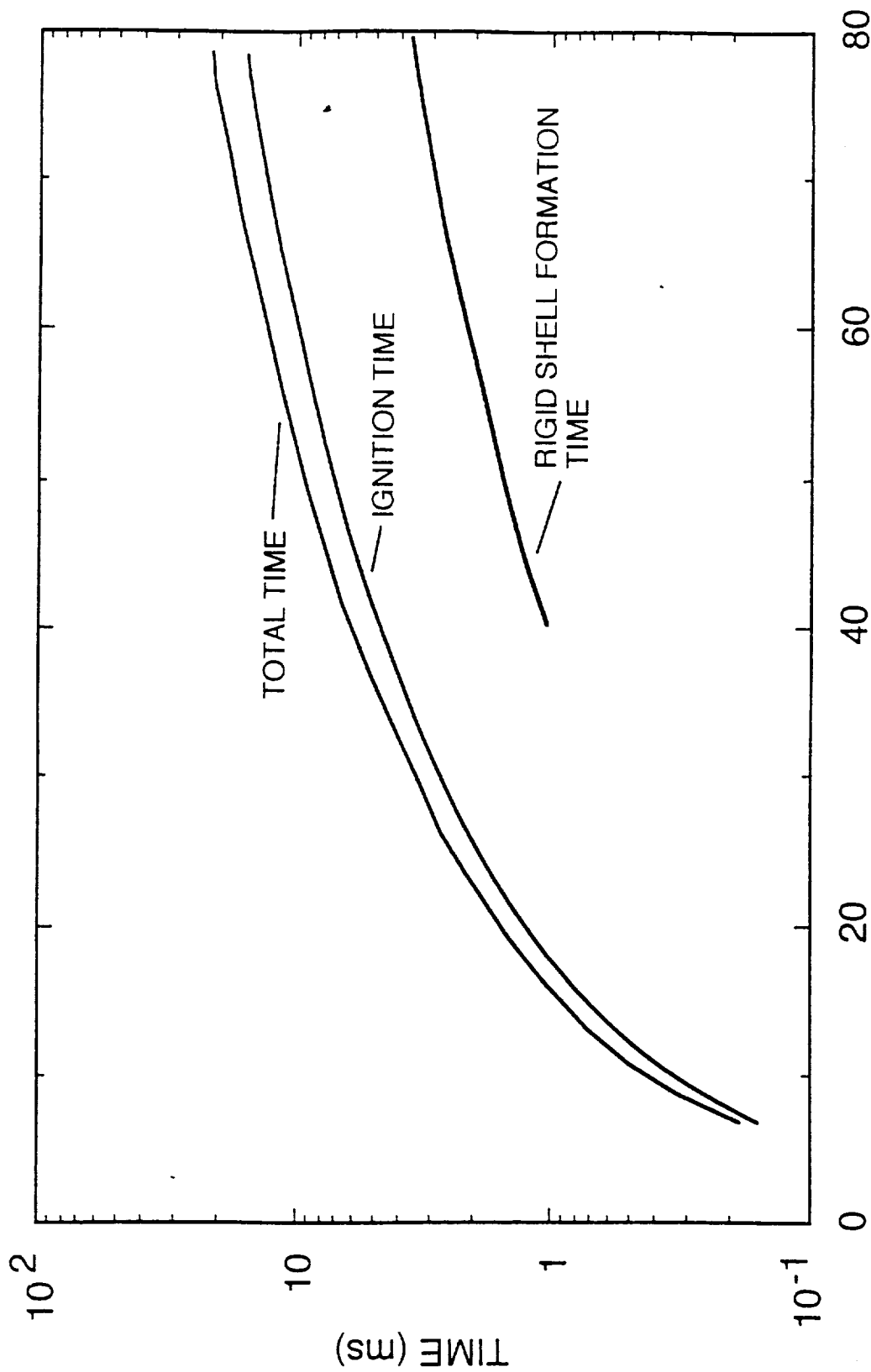
COMPARISON OF EXPERIMENTAL AND THEORETICAL RESULTS

Assuming that particles travel at an average velocity of 7 m/s and that droplet life histories begin 5 mm above the burner instead of at the burner face, as discussed above, then the mean particle time-of-flight can be estimated for each measurement location. Particles will reach the 10 mm axial location in 0.71 ms, and the 15 mm location in 1.4 ms. It is important to note that these calculated times-of-flight are highly sensitive to the location at which droplet activity begins. With these assumptions, experimental results correlate reasonably well with present and prior theoretical analyses.^{11,12} Calculations based on the analysis of Refs.^{11,12} are presented in Fig. 12. This figure shows three theoretical times: the time required to form a rigid shell, the time to agglomerate ignition,¹¹ and the total time to completion of agglomerate combustion,¹² all shown as functions of initial droplet diameter.

Figure 10c ($x = 10$ mm) shows that aluminum combustion occurs for some particles in the 5-10 μm size range. The time for a particle to reach this point should be comparable to calculated agglomerate ignition times. Figure 12 indicates that a 14.3 μm slurry droplet, forming a 10 μm agglomerate, would require 0.6 ms for aluminum combustion to begin, agreeing favorably with the above experimental information.

Since rigid shell formation is a precursor to secondary atomization, it seems that calculated times for rigid shell formation are approximately equal to disruption times if the shell sealing interval is short. Figure 12 indicates that a 40 μm slurry droplet should form a rigid shell in 0.95 ms. This time span of 0.95 ms falls between the

ALUMINUM SLURRY IGNITION AND COMBUSTION TIMES
FOR METHANE WITH 60% OXYGEN, AMBIENT TEMP 2653 K



SLURRY DROPLET INITIAL DIAMETER (μm)

FIGURE 12. Theoretical total combustion time, aluminum agglomerate ignition time, and rigid shell formation time, all as functions of initial droplet diameter.

particle times-of-flight required to reach the 10 mm location ($t=0.71$ ms), and the 15 mm location ($t=1.4$ ms). The sharp decrease in particle number in the 20-40 μm range seen in Fig. 10d ($x = 15$ mm) occurs in this same region. It is interesting to note that the lower end of this size range, 20 μm , is less than the predicted minimum diameter, $d_{o,lim}=34.7$ μm , for a rigid shell to form.

This discrepancy between experimental and theoretical minimum diameters could be due to experimental uncertainty in measuring particle size, primarily associated with the unknown slurry droplet index of refraction. However, the intensity of scattered light in the near-forward direction is known to be relatively insensitive to the particle index of refraction. Calculations show that increasing the index of refraction from 1.1 to 2.0 results in a maximum increase of 5 μm in size for a given scattered intensity. Another reason for this discrepancy could be that the limiting diameter, $d_{o,lim}$, is highly sensitive to the critical shell thickness for rigid shell formation. The predicted minimum diameter, $d_{o,lim}= 34.7$ μm , discussed in a previous section, was calculated assuming a critical shell thickness of three ultimate particles, following the work of Lee and Law.⁷ If this critical thickness is instead assumed to be only two ultimate particles, then the predicted $d_{o,lim}$ becomes 24 μm , which is within the range of experimentally measured limiting diameters of 20-25 μm .

If the critical shell thickness for our slurries is indeed smaller than that of Lee and Law,⁷ this difference could be a consequence of how surfactants or particle morphology affecting particle binding. The critical shell thickness of $3 d_u$ was determined using a carbon slurry ($d_u = 0.3$ μm) containing unknown surfactants and stabilizers.⁷ Since these additives are likely to be different in type and concentration from those in the aluminum slurry used in these experiments, it is reasonable to assume that the shell formation characteristics are different. Measurements of ultimate

particle size and shape in similar aluminum slurries, by Stearns et al,⁵ indicate that a range of particle sizes and shapes are present. These variations in particle size and shape may result in binding between particles due to smaller particles wedging in between the larger particles and particles snagging on each other. If the ultimate particles in the carbon slurry were more uniform in size or smoother in shape, the shell formation characteristics could again be altered.

CONCLUSIONS

Based on the above theoretical and experimental results, the following conclusions can be drawn for aluminum/liquid hydrocarbon propellants:

1. Increasing solids mass fractions and decreasing ultimate particle diameter are predicted to significantly decrease the minimum slurry droplet diameter required to form a rigid shell. Since rigid shell formation is a precursor to secondary atomization, effects that reduce the minimum droplet diameter capable of forming a rigid shell should also reduce the minimum diameter required for secondary atomization.
2. Calculations show that slurry droplets close to the minimum diameter for rigid shell formation should contain little or no liquid slurry after shell sealing. This lack of free slurry may reduce the effectiveness of droplet disruption since only shell fragments, rather than secondary slurry droplets, are produced. In contrast, larger droplets contain a significant amount of liquid slurry after a sealed shell is formed. Disruptive burning of these large droplets should lead to beneficial secondary atomization.
3. For small droplets ($d_0 < 50 \mu\text{m}$), shell stress is predicted to increase at essentially the same rate, regardless of the shell sealing time, as a consequence of constant shell thickness. In contrast, the stress in larger droplets was found to increase more rapidly for earlier sealing times since the shells are thinner at these shorter times, indicating that short sealing times may lead to rapid droplet disruption and secondary atomization.

4. Calculated agglomerate ignition times were found to be in reasonable agreement with experimental results. However, time-of-flight calculations are highly sensitive to the position at which droplet activity is assumed to begin, making exact comparisons uncertain.

5. Theoretical calculations, based on a critical rigid shell thickness of three particles, predict a larger minimum slurry droplet diameter ($d_{o,lim} = 34.7 \mu\text{m}$) required for disruption than was observed in the experimental data ($d_{o,lim} = 20 \mu\text{m}$). This could be due to experimental uncertainties associated with the unknown slurry particle index of refraction or may be due to difficulties in determining the critical shell thickness required for rigid shell formation.

FUTURE PLANS

Plans for the next six months include the following:

1. Develop imaging techniques to complement the existing experimental apparatus and to provide time resolved visualization of the secondary atomization process.
2. Collect droplet samples at various points in the droplet stream and use a scanning electron microscope to examine shell characteristics.
3. Model and calculate the development of droplet size distributions as a function of axial distance above the burner, including secondary atomization effects.
4. Begin development of a one-dimensional rocket engine model using aluminum slurry. This model will ultimately include the effects of radiation heat transfer, two-phase flow losses, and secondary atomization.
5. Examine the role of surfactants in secondary atomization by adding additional surfactants to existing slurries.
6. Continue investigating the sample volume size probability distribution function and its sensitivity to particle index of refraction.

ACKNOWLEDGEMENT

We would like to acknowledge the work done by Dave Yoset on the analytical analysis of the aluminum agglomerate ignition and combustion process.

REFERENCES

- 1 Turns, S.R., Mueller, D. C., and Scott, M. J., "Ignition and Combustion of Metallized Propellants - Semi-Annual Report," Grant No. NAG-3-1044, January 1990.
- 2 Turns, S.R., Mueller, D. C., and Scott, M. J., "Ignition and Combustion of Metallized Propellants - Semi-Annual Report," Grant No. NAG-3-1044, July 1990.
- 3 Mueller, D. C., Scott, M. J., and Turns, S.R., "Ignition and Combustion of Metallized Propellants - Semi-Annual Report," Grant No. NAG-3-1044, January 1991.
- 4 Rapp, D.C., and Zurawski, R.L., "Characterization of Aluminum/RP-1 Gel Propellant Properties," AIAA Paper 88-2821, July 1988.
- 5 Stearns, R.S., and Hall, L.W., Jr., "Aluminum Slurry Fuel Formulation and Combustion," AFWAL-TR-88-2052, Nov. 1988.
- 6 Wong, S.-C., Lin, A.-C., and Chi, H.-Y., "Effects of Surfactant on the Evaporation, Shell Formation, and Disruptive Behaviors of Slurry Droplets," *Twenty-Third Symposium (International) on Combustion*, The Combustion Institute, Pittsburgh, 1990, pp. 1391-1397.
- 7 Lee, A., and Law, C.K., "Gasification and Shell Characteristics in Slurry Droplet Burning," *Combust. Flame*, Vol. 85, 1991, pp. 77-93.
- 8 Takahashi, F., Dryer, F.L., and Williams, F.A., "Combustion Behavior of Free Boron Droplets," *Twenty-First Symposium (International) on Combustion*, The Combustion Institute, Pittsburgh, 1986, pp. 1983-1991.
- 9 Takahashi, F., Heilweil, I.J., and Dryer, F.L., "Disruptive Burning Mechanism of Free Slurry Droplets," *Combust. Sci. and Tech.*, Vol. 65, 1989, pp. 151-165
- 10 Cho, S.Y., Takahashi, F., and Dryer, F.L., "Some Theoretical Considerations on the Combustion and Disruption of Free Slurry Droplets," *Combust. Sci. and Tech.*, Vol. 67, 1989, pp. 37-57.
- 11 Wong, S.-C., and Turns, S.R., "Ignition of Aluminum Slurry Droplets," *Combust. Sci. and Tech.*, Vol. 52, 1987, pp. 222-242.
- 12 Turns, S.R., Wong, S.-C., and Ryba, E., "Combustion of Aluminum-Based Slurry Agglomerates," *Combust. Sci. and Tech.*, Vol. 54, 1987, pp. 299-318.
- 13 Wong, S.-C., and Turns, S.R., "Disruptive Burning of Aluminum/Carbon Slurry Droplets," *Combust. Sci. and Tech.*, Vol. 66, 1989, pp. 75-92.
- 14 Kuo, K.K., *Principles of Combustion*, John Wiley & Sons, New York, 1986, pp. 370-385.

- 15 Luikov, A.V., *Heat and Mass Transfer in Capillary-porous Bodies*, Pergamon Press, Oxford, 1966.
- 16 Luikov, A.V., and Mikhaylov, Y.A., *Theory of Energy and Mass Transfer*, Prentice-Hall, Inc., Englewood Cliffs, 1961.
- 17 Reid, R.C., Prausnitz, J.M., and Poling, B.E., *The Properties of Gases and Liquids*, 4th Ed., McGraw-Hill, New York, 1987.
- 18 Szekely, G.A., Jr. "Experimental Evaluation of a Carbon Slurry Droplet Combustion Model," Ph.D. Thesis, The Pennsylvania State University, 1982.
- 19 Brzustowski, T.A., and Glassman, I., "Vapor-Phase Diffusion Flames in the combustion of Magnesium and Aluminum: II - Experimental Observations in Oxygen Atmosphere," *Progress in Astronautics and Aeronautics*, 15:117, AIAA, Academic Press, NY.
- 20 Rautenberg, T.H., Jr., and Johnson, P.D., "Light Production in the Aluminum-Oxygen Reaction," *Journal of the Optical Society of America*, 50:602-606, 1960.
- 21 Wang, J.C.F., and Hencken, K.P., "In Situ Particle Size Measurements Using a Two-Color Laser Scattering Technique," *Applied Optics*, 25:653-657, 1986.
- 22 Holve, D.J., Tischner, D., Wang, J.C.F., and Hardesty, D.R., "Design Criteria and Recent Developments of Optical Single Particle Counters for Fossil Fuel Systems," *Optical Engineering*, 20:529-539, 1981.

